Analytical and Bioanalytical Chemistry
https://doi.org/10.1007/s00216-018-0893-1

RESEARCH PAPER

An ultrasensitive hollow-silica-based biosensor for pathogenic *Escherichia coli* DNA detection

Eda Yuhana Ariffin[1] · Yook Heng Lee[1,2] · Dedi Futra[3] · Ling Ling Tan[2] · Nurul Huda Abd Karim[1] · Nik Nuraznida Nik Ibrahim[4] · Asmat Ahmad[4]

Received: 27 November 2017 / Revised: 31 December 2017 / Accepted: 16 January 2018

Abstract
A novel electrochemical DNA biosensor for ultrasensitive and selective quantitation of *Escherichia coli* DNA based on aminated hollow silica spheres (HSiSs) has been successfully developed. The HSiSs were synthesized with facile sonication and heating techniques. The HSiSs have an inner and an outer surface for DNA immobilization sites after they have been functionalized with 3-aminopropyltriethoxysilane. From field emission scanning electron microscopy images, the presence of pores was confirmed in the functionalized HSiSs. Furthermore, Brunauer–Emmett–Teller (BET) analysis indicated that the HSiSs have four times more surface area than silica spheres that have no pores. These aminated HSiSs were deposited onto a screen-printed carbon paste electrode containing a layer of gold nanoparticles (AuNPs) to form a AuNP/HSiS hybrid sensor membrane matrix. Aminated DNA probes were grafted onto the AuNP/HSiS-modified screen-printed electrode via imine covalent bonds with use of glutaraldehyde cross-linker. The DNA hybridization reaction was studied by differential pulse voltammetry using an anthraquinone redox intercalator as the electroactive DNA hybridization label. The DNA biosensor demonstrated a linear response over a wide target sequence concentration range of 1.0×10^{-12}–1.0×10^{-2} μM, with a low detection limit of 8.17×10^{-14} μM (R^2 = 0.99). The improved performance of the DNA biosensor appeared to be due to the hollow structure and rough surface morphology of the hollow silica particles, which greatly increased the total binding surface area for high DNA loading capacity. The HSiSs also facilitated molecule diffusion through the silica hollow structure, and substantially improved the overall DNA hybridization assay.

Keywords Electrochemical DNA biosensor · *E. coli* DNA detection · Hollow silica spheres · Immobilization · Hybridization

Introduction

Escherichia coli bacteria are commonly found in the intestines of humans and animals. Most *E. coli* strains are harmless; however, some serotypes are pathogenic, such as *E. coli* O157:H7, which produces Shiga toxin and causes severe illnesses (e.g. stomach cramps, diarrhoea, kidney failure) and even death [1]. Shiga toxin-producing *E. coli* can be transmitted through contaminated water or food, or through contact with infected animals or people. The symptoms of *E. coli* infection usually start within 3 or 4 days after exposure, but the incubation period can be as short as 1 day or as long as 10 days.

Traditional microbiological detection of *E. coli* involves differential agar media for bacterial colony growth followed by enumeration of *E. coli* bacteria on the basis of colony-forming units. Preenrichment of the sample with selective culture, biochemical screening and serological confirmation are essential [2]. Although these methods are sensitive and selective, it takes days or weeks to get results. Moreover, the process is laborious and requires well-trained personnel, and interpretation of the test results is difficult [3]. The culture-based method is vulnerable to microbial contamination, and frequently results in inhibition of growth of the bacteria of

✉ Yook Heng Lee
leeyookheng@yahoo.co.uk

[1] School of Chemical Sciences and Food Technology, Faculty of Science and Technology, Universiti Kebangsaan Malaysia, UKM, 43600 Bangi, Selangor Darul Ehsan, Malaysia

[2] Southeast Asia Disaster Prevention Research Initiative, Institute for Environment and Development, Universiti Kebangsaan Malaysia, 43600 Bangi, Selangor Darul Ehsan, Malaysia

[3] Department of Chemistry Education, Faculty of Education, Universitas Riau, Pekan Baru, Riau 28131, Indonesia

[4] School of Biosciences and Biotechnology, Faculty of Science and Technology, Universiti Kebangsaan Malaysia, 43600 Bangi, Selangor Darul Ehsan, Malaysia

Published online: 05 March 2018

interest as well as the presence of viable but non-culturable bacteria, which leads to the underestimation of viable cells of the pathogen from water [3]. *E. coli* genotype detection can be conducted with DNA colony blot hybridization, but a long handling time makes this method unsuitable for most laboratory diagnoses [4]. Detection of bacteria has evolved to more rapid, sensitive and specific immunoassays such as the enzyme-linked immunosorbent assay (ELISA) and polymerase chain reaction methods, but these methods are limited by the requirements of sophisticated instruments and pretreatment involving purification of the samples [5]. Finally, this method uses agarose electrophoresis gel stain, but the process is time-consuming and dangerous [6]. The ELISA technique needs overnight incubation and 2 h to perform the test [7]. The plate counting method, ELISA and polymerase chain reaction need enrichment, separation, a morphology test, a serological test and a biochemical test to detect the exact pathogen [8]. Use of a DNA biosensor is a suitable method to solve this problem because DNA biosensors are easy to handle, portable and highly sensitive.

In recent years, DNA biosensors based on nucleic acid hybridizations have been vigorously pursued. Various analytical biosensing methods have been used for the quantification of DNA, including optical methods [9], magnetic methods [10], use of field-effect transistors [11], use of a quartz crystal microbalance [12] and electrochemical techniques [13]. The electrochemical DNA biosensor method has received the most attention because of its high sensitivity, short reaction time, convenience and simple operation [14]. Li et al. [15] used the electrochemical DNA biosensor method to detect DNase I activity through the presence of methylene blue on a gold electrode. Evtugyn et al. [16] constructed electrochemical DNA sensors based on nanostructured organic dye/DNA/polyelectrolyte complexes. However, the sensitivity of these sensors has remained low and the concentration of the target gene is usually very low in the samples. Therefore, an ultrasensitive analytical method of detecting nucleic acids is clearly essential [17]. Generally, the sensitivity of the DNA biosensor chiefly relies on the structure and surface morphology of the DNA supporting material. The use of large surface area materials such as microparticles or nanoparticles has often allowed more DNA probes to be immobilized on the matrix so as to increase the biosensor sensitivity compared with that of a one-dimensional structure membrane [18].

Electrochemical biosensors based on silica nanoparticles are widely used as a biomolecule supporter to detect the DNA hybridization reaction. Liebana et al. [19] used silica magnetic particles as the carrier in electrochemical genosensing of *Salmonella*, *Listeria* and *E. coli*. The genosensor had a low detection limit of less than 0.15 ng μL^{-1}. Cai et al. [20] used silica nanoparticles with a carboxyl group to develop a biosensor for adenosine triphosphate-binding aptamer detection. Hoechst 33258 was used as the hybridization label. The biosensor had a low detection limit of less than 20 μM. Cha et al. [21] developed a hepatitis B virus DNA biosensor by using silica nanoparticles with a carboxyl group. This DNA biosensor used ethyl-3-(3-dimethylaminopropyl)carbodiimide and *N*-hydroxysuccinimide to activate the carboxyl functional group. It was highly sensitive, was stable, had high reproducibility and had a low detection limit.

Hollow silica appears to be attractive because of its high chemical and thermal stability, large surface area and tunable size, and good compatibility with other materials [22–24]. It has a wide range of applications, including as a catalyst support [25], gas adsorbent [26], heavy metal ion adsorbent [27], inorganic carrier [28] and semiconductor nanoparticles [29, 30]. Besides, hollow silica has also been used as an efficient supporting substrate for enzyme immobilization [31, 32] and for drug or small interfering RNA delivery applications [24, 33]. It has great potential to be a good DNA supporter candidate by virtue of its large inner and outer surfaces, which can be differentially functionalized. In addition, its inner void allows diffusion of small molecules and ions, providing a shorter diffusion path length [22, 34]. A higher surface area is available for DNA probe immobilization for the same spot diameter compared with a flat surface [14].

Because of the large surface area provided by hollow silica spheres (HSiSs), we have studied the potential of this material for improving DNA biosensor performance. In preliminary investigations on the synthesis and characterization of HSiSs, we studied this material by Fourier transform IR spectroscopy and cyclic voltammetry (CV) [35]. In the work reported here, we further investigated the structure and also the potential of a DNA biosensor constructed by our depositing a gold nanoparticle (AuNP)/HSiSs matrix on a screen-printed carbon paste electrode for ultrasensitive detection of *E. coli* DNA. We obtained the *E. coli* pathogenic DNA sequences from Solanki et al. [36]. The 3-aminopropyltriethoxysilane (APTES)-functionalized HSiSs were synthesized with use of Tween 20 surfactant molecules, which formed the spherical micelle template. The three-dimensional silica network was formed around the surfactant micelle template via hydrolysis and condensation of silicon alkoxide precursors. The core–shell compositions then underwent thermal decomposition to remove the surfactant template. The aminated DNA probe was coupled to the aminated HSiSs via a glutaraldehyde bifunctional cross-linker, and deposited onto the AuNP-modified screen-printed carbon paste electrode. The AuNPs were used to increase the conductivity of the DNA biosensor. *E. coli* target DNA was quantified by differential pulse voltammetry (DPV) in the presence of an electroactive anthraquinone DNA hybridization label.

Materials and methods

Instrumentation

CV and DPV were performed with an Autolab PGSTAT electrochemical analysis system supplied with the GPES software package. The working electrode was prepared by modification of the screen-printed carbon paste electrode (Scrint Technology, Malaysia) with HSiSs, AuNPs and DNA molecules. The auxiliary electrode was a platinum electrode, and a Ag/AgCl reference electrode was used to measure the potential of the working electrode. All DPV electrochemical measurements were performed in 6 mL of 0.05 M potassium phosphate buffer at pH 7.

Chemicals

APTES (98%), glutaraldehyde, AuNP powder (less than 100 nm) and synthetic oligonucleotides (Table 1) were supplied by Sigma-Aldrich. Tetraethyl orthosilicate (98%), Tween 20 surfactant, sodium fluoride (98.5%) and anthraquinone-2-sulfonic acid monohydrate salt (AQMS) were purchased from Fluka, R & M Chemicals, Merck and Acros, respectively. Deionized water was used for preparation of all aqueous solutions. A stock solution of DNA probe was prepared in 0.05 M potassium phosphate buffer (pH 7), and complementary DNA (cDNA) solution was prepared in 0.05 M potassium phosphate buffer containing 0.1 M KCl at pH 7. The pathogenic sequences chosen were acquired from Solanki et al. [36].

Synthesis and characterization of aminated HSiSs

HSiSs were synthesized according to the method reported by Boissiere et al. [37] with some modifications. Firstly, tetraethyl orthosilicate and Tween 20 were mixed in a molar ratio of 8:1 for 10 min on a magnetic stirrer (IKA 9500100 C-Mag HS7) followed by addition of 0.748 g of sodium fluoride to the mixture and stirring for another 3.5 h. The mixture was then incubated in a shaking water bath at 27 °C for 8 days. The resulting precipitate was sequentially washed with ethanol and deionized water by centrifugation at 4000 rpm for 15 min each. The resultant HSiSs were finally oven-dried at 200 °C for 6 h and calcined in air at 620 °C for 6 h. Next, the as-synthesized HSiSs were treated with 2 mL of APTES (98%) with overnight stirring, and air-dried for 24 h. The size and morphology of the aminated HSiSs were determined by field emission scanning electron microscopy (FESEM). The Brunauer–Emmett–Teller (BET)/Barret–Joyner–Halenda method and X-ray diffraction (XRD) were used to analyse the pores. The BET/Barret–Joyner–Halenda analysis was used to explain the physical absorption of gas molecules onto the solid surface and was used as the basic analytical technique to measure the material specific area. BET theory refers to the absorption of a gas such as nitrogen, argon and carbon dioxide onto several layers to determine surface area data. BET analysis was performed to analyse the silica pores. A particle size analyser was used for HSiS characterization. About 5 mg of dried APTES-functionalized HSiSs was dispersed in 500 μL of 30% ethanol for further use in DNA biosensor fabrication.

Table 1 The DNA oligonucleotide sequences used in the present research

DNA	Base sequences
DNA probe	5′-GGTCCGCTTGCTCTCGC [AmC3]
cDNA	5′-GCGAGAGCAAGCGGACC-3′
ncDNA	5′-CTAGTCGTATAGTAGGC-3′

cDNA complementary DNA, *ncDNA* non-complementary DNA

Fabrication of the DNA biosensor

The screen-printed carbon paste electrode was first modified with AuNPs by deposition of 10 μL of colloidal AuNPs in 30% ethanol onto the active surface of the screen-printed electrode (SPE) and air-dried at room temperature (27 °C). About 4 μL of aminated HSiS suspension in ethanol was then deposited onto the AuNP-modified SPE (AuNP-SPE), and allowed to dry under ambient conditions, followed by immersion in 8% glutaraldehyde for 1 h, and subsequent soaking in 300 μL of 1 μM DNA probe solution overnight. These pathogenic DNA sequences were obtained from Solanki et al. [36]. After overnight immersion, the resulting DNA biosensor was carefully rinsed with 0.05 M potassium phosphate buffer (pH 7) to remove the unbound DNA probe. DNA hybridization was performed by the dipping of the DNA biosensor in 300 μL of target DNA solution for 1 h at 27 °C. The DNA biosensor was then rinsed again with 0.05 M potassium phosphate buffer at pH 7 to remove the excess cDNA fragments, followed by immersion in 1 mM AQMS solution for 40 min before the DNA biosensor response was investigated by means of DPV. The stepwise fabrication of the aminated HSiS-based electrochemical DNA biosensor is depicted in Fig. 1. The electrochemical behaviour of each immobilized substance layer deposited on the SPE was characterized by CV at a scan rate of 100 mVs^{-1} with use of 1 mM potassium ferricyanide [$K_3Fe(CN)_6$] redox indicator.

Optimization of DNA biosensor response for DNA in pathogenic *E. coli* detection

The amounts of AuNPs and aminated HSiSs deposited on the SPE were optimized by our varying the AuNP and aminated HSiS loadings from 0.016 to 0.096 mg and from 0.01 to 0.05

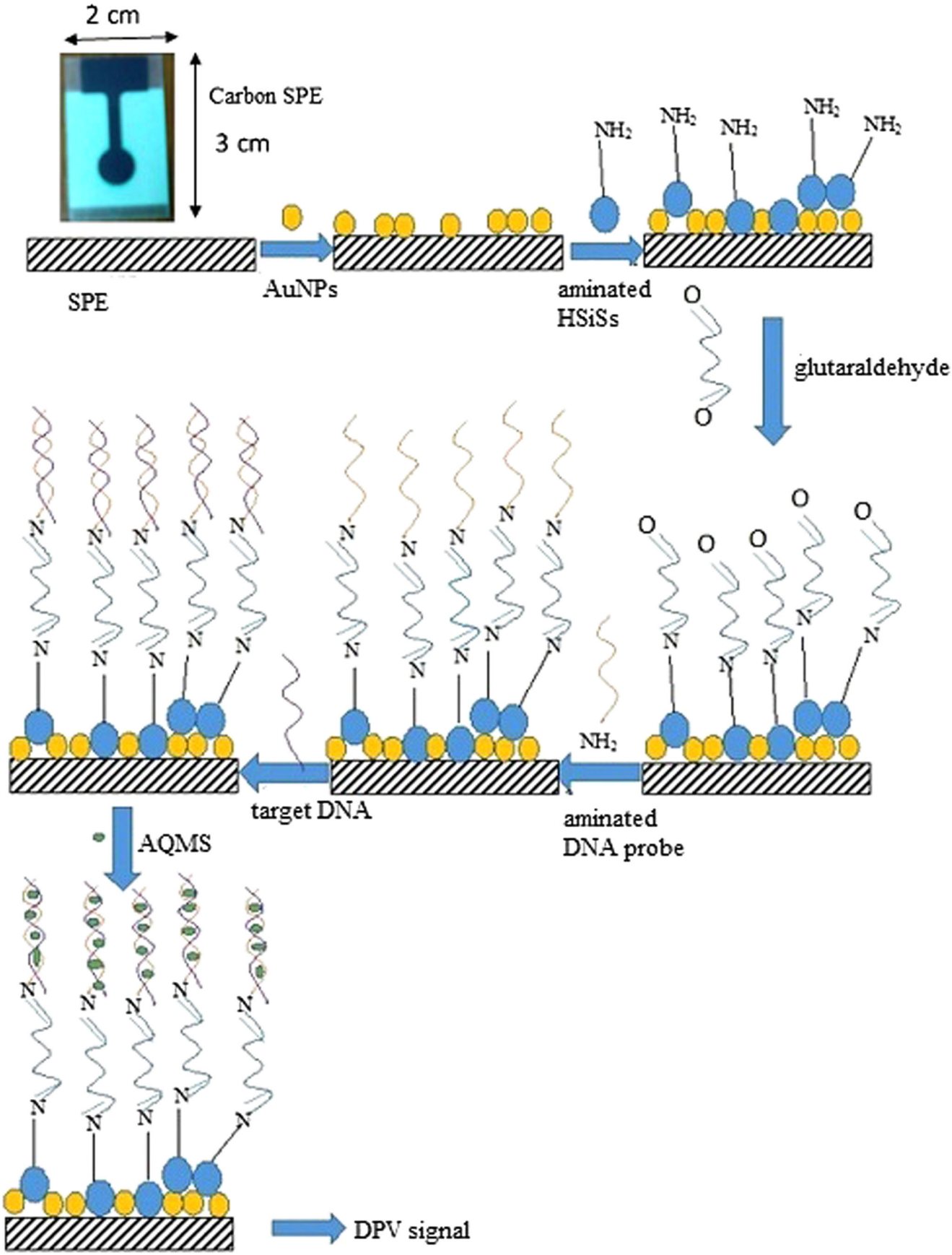
2 cm
Carbon SPE
3 cm
SPE
AuNPs
NH2
aminated
HSiSs
O
glutaraldehyde
target DNA
aminated
DNA probe
AQMS
DPV signal

◀ **Fig. 1** The stepwise fabrication of the aminated hollow silica sphere (HSiS)-based electrochemical DNA biosensor. AQMS anthraquinone-2-sulfonic acid monohydrate salt, AuNPs gold nanoparticles, DPV differential pulse voltammetry, SPE screen-printed electrode

mg, respectively. DNA probe loading, on the other hand, was evaluated between 0.2 and 5 μM, while the amounts of AuNPs and aminated HSiSs on the SPE were kept constant at 0.08 and 0.04 mg, respectively,. DNA hybridization was performed with 1×10^{-8} μM cDNA in 0.05 M potassium phosphate buffer containing 0.1 M KCl at pH 7 followed by an intercalation reaction with 1 mM AQMS. Sodium phosphate, potassium phosphate and tris(hydroxymethyl)aminomethane hydrochloride buffers of 0.05 M and pH 7 were prepared to determine the suitability of the buffer type for the optimal DNA hybridization reaction. The effect of DNA hybridization buffer pH was investigated with 0.05 M potassium phosphate buffer in the pH range from 5 to 9. To investigate the effect of the buffer concentration, the potassium phosphate buffer (pH 7) concentration was varied between 0.005 and 0.07 M. The ionic strength of the DNA hybridization buffer was studied with various concentrations of KCl (0.01–0.2 M) in 0.05 M potassium phosphate buffer at pH 7. The DNA probe immobilization was performed over a period of 1–24 h, and the DNA hybridization time was determined by exposure of the DNA biosensor to target DNA for 20–160 min. The calibration curve of the DNA biosensor was established with a series of cDNA concentrations from 1×10^{-14} to 1×10^{-2} μM; this was done in triplicate. The selectivity of the DNA biosensor was examined with cDNA and non-complementary DNA of the same concentration. The reversibility of the DNA biosensor was studied by our alternately incubating the DNA biosensor in 1×10^{-8} μM cDNA (30 min) and 0.1 M NaOH (15 min), with the DPV measurement taken after each incubation.

Sample testing and confirmation

The amperometric *E. coli* DNA biosensor was then validated and compared against the standard plating method according to the FDA's Bacteriological Analytical Manual for *E.coli* determination in water samples. Water samples were collected from various locations along Langat River. After prefiltration of samples through a 45-μm pore size filter to remove large particles, 100 mL of each water sample was filtered through a 0.2-μm pore size, 100-grid membrane filter. After filtering, the numbers of *E. coli* from each sample were determined by culture on eosin methylene blue agar. For DNA biosensor testing, all samples were heated and sonicated for 20 min to obtain the DNA of bacteria [38, 39]. The *E. coli* DNA biosensor electrode was immersed in the water sample for DNA hybridization for 1 h, and 1 mM AQMS was added as a redox label before the biosensor response was measured.

Results and discussion

Morphology and characterization of aminated HSiSs and electrochemical response of the modified SPE

Figure 2a shows FESEM micrographs of the aminated HSiSs with dimensions in the 50–200-μm size range and a circular pore with pore diameter less than 1 μm; Fig. 2b shows an FESEM micrograph of the non-hollow silica spheres. The inner and outer rough surfaces of the APTES-modified HSiSs increased the binding surface area, resulting in high DNA immobilization capacity.

Nitrogen gas absorption characterization is a technique to analyse the texture properties of HSiSs such as pore volume, specific surface area and pore size distribution. Measurements based on nitrogen absorption and desorption were performed at 77 K. Nitrogen gas absorption is an IUPAC method for porous materials with specific surface area greater than 5 m^2 g^{-1} [40]. According to Zielinski and Kettle [41], porous materials have a larger BET surface area than materials without pores. BET analysis of HSiSs showed that the BET surface area is 302.6976 m^2 g^{-1}, with a pore area of 5.1887 m^2 g^{-1} and a pore volume of 1.927×10^{-3} cm^3 g^{-1}. BET analysis of non-hollow silica spheres showed that the BET surface area is 76.7881 m^2 g^{-1}, with a pore area of 1.85 m^2 g^{-1} and a pore volume of 1.045×10^{-3} cm^3 g^{-1}.

A particle size analyser was used to determine the size and surface charge properties of the HSiSs. Most of the HSiSs had a diameter of around 220.2 nm. The HSiSs had a zeta potential of -0.75 mV. This means the HSiSs were negatively charged. The diameter of the HSiSs increased to 430.8 nm and the HSiSs were positively charge (6.76 mV) after silica had been functionalized with APTES. Normally, silica is negatively charged because of the silanol group, and after APTES addition, silica is positively charged because of the amine group in the silica chain.

XRD analysis was performed to obtain the structure of the silica spheres. Figure 3 shows the XRD spectrum after calcination. The clear and broad spectral peaks at 2θ around 13° and 23° showed that the synthesized HSiSs were in the amorphous form and that no crystal structure has been formed [42]. These HSiSs were similar in structure to nanosilica and mesoporous silica [43, 44]. The low absorption peak at $2\theta = 4°$ showed that the silica spheres were hollow or porous [45].

The electrochemical properties of the AuNP-SPE and the HSiS-modified SPE (HSiS-SPE) were examined by CV with potassium ferricyanide as a redox-active test probe, and were compared with the electrochemical behaviours of the bare SPE, AuNP-SPE and HSiS-SPE (Fig. 4). The sigmoidal voltammetric responses of the modified SPEs suggest the predominance of radial diffusion instead of the classical linear mode of mass transfer at millimetre-sized electrodes [46]. On the basis of the electrochemical data in Table 2, the

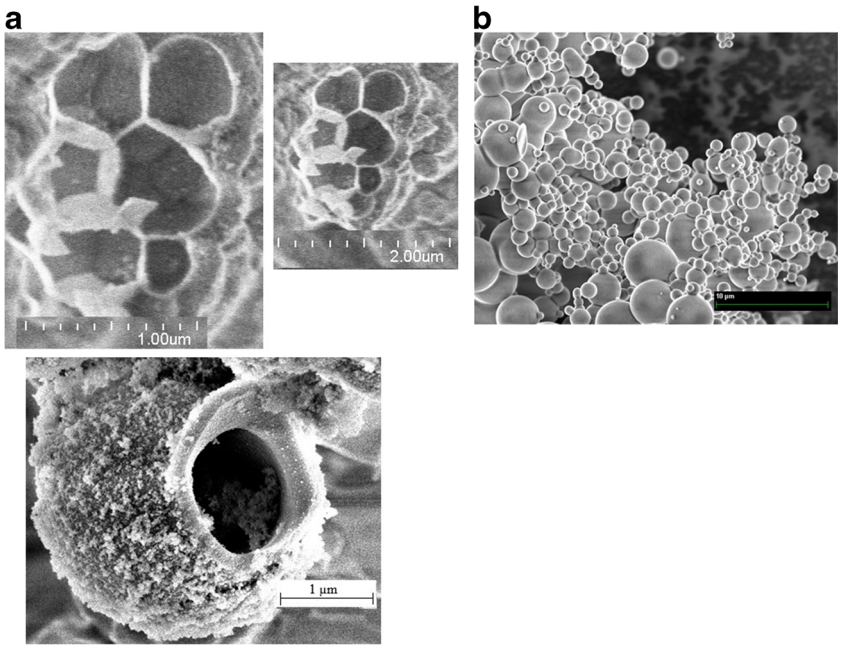

Fig. 2 **a** Field emission scanning electron microscopy (FESEM) micrographs of the aminated hollow silica spheres. **b** FESEM micrograph of the non-hollow silica spheres

potential difference (ΔE_p) increased in the electrode order of AuNP/HSiS-modified SPE (AuNP/HSiS-SPE)<AuNP-SPE<bare SPE<HSiS-SPE as the electron transfer rate decreased at the electrode surface in the electrode order of AuNP/HSiS-SPE>AuNP-SPE>bare SPE>HSiS-SPE. Both the bare SPE and the HSiS-SPE exhibited larger separation in peak potentials because of the rather inferior electron conductivity of the carbon paste material itself and the non-conductive characteristic of the aminated HSiSs, respectively, which reduced the electron transport efficiency on the electrode surface. However, when the AuNP-SPE was doped with aminated HSiSs to form a hybrid conductor material, it exhibited high electron transfer performance, which was due to the high electrical conductivity of the AuNPs and efficient diffusion of redox-active moieties through the aminated HSiSs [47]. In addition, the anodic to cathodic peak current ratio (I_{PA}/I_{PC}) of the AuNP/HSiS-SPE was near 1, which means that the reversible redox system was still maintained with the hybrid electrode.

Figure 5 shows the DPV response of the SPE and modified SPEs with an anthraquinone oligonucleotide label as the redox indicator. The strong and sharp AQMS DPV peak current response at -0.5 V indicates that the AQMS redox probe had been intercalated into the immobilized DNA double helix on the

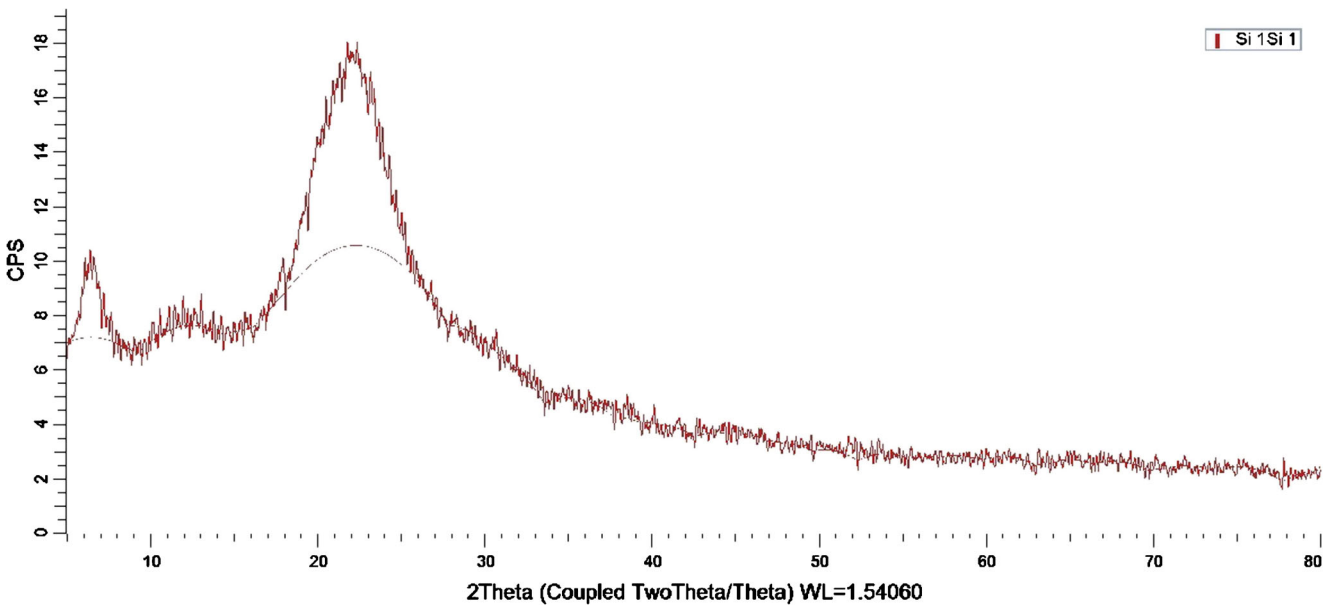

Fig. 3 X-ray diffraction spectrum after calcination

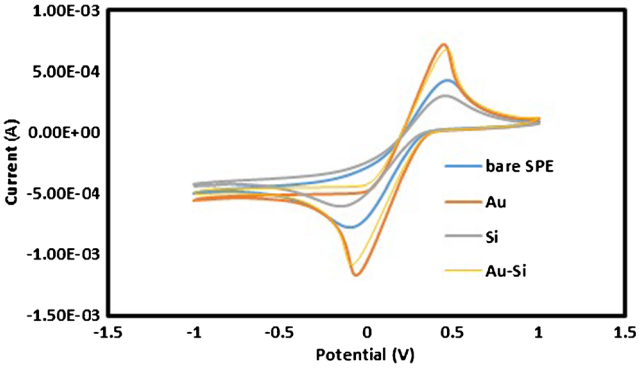

Fig. 4 Cyclic voltammograms of 1 mM $K_3Fe(CN)_6$ redox indicator obtained with the bare screen-printed electrode (SPE), gold nanoparticle (AuNP)-modified SPE, hollow silica sphere (HSiSs)-modified SPE and AuNP/HSiS-modified SPE at a scan rate of 100 mVs^{-1}

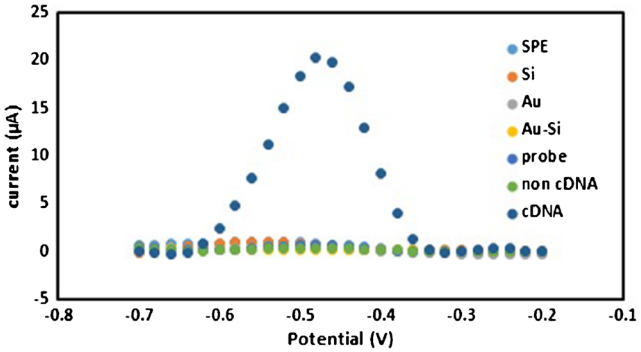

Fig. 5 Differential pulse voltammograms of the screen-printed electrode (SPE) and modified SPEs in 0.05 M potassium phosphate buffer (pH 7) with 1 mM anthraquinone-2-sulfonic acid monohydrate salt as the indicator. cDNA complementary DNA

HSiS/AuNP-SPE after the probe–target hybridization reaction. This suggests that the DNA probes had been successfully immobilized on the aminated HSiSs via covalent cross-linking with glutaraldehyde [48, 49]. No observable AQMS DPV response at -0.5 V was obtained with the immobilized single-stranded DNA probe before and after hybridization with non-complementary DNA. This was attributed to the electrostatic repulsion force between AQMS and the DNA-modified HSiS/AuNP-SPE of the same charge. Furthermore, the DNA electrode based on the HSiS/AuNP hybrid substrate showed 100% complementary with the target sequence, which implies a superior selectivity of the proposed DNA biosensor toward the detection of *E. coli* cDNA. The bare SPE, AuNP-SPE, HSiS-SPE and HSiS/AuNP-SPE gave negligible DPV responses to AQMS, which indicates there was no specific adsorption of AQMS on the electrode surface.

Optimization of AuNP, aminated HSiS and DNA probe loadings on the SPE

As the non-conductive aminated HSiSs were used as the carrier matrix for DNA immobilization, AuNPs were added to facilitate the electron transfer from the intercalated AQMS DNA hybridization redox label to the SPE surface. On increase of the amount of AuNPs from 0.016 to 0.08 mg, the DNA biosensor response increased appreciably because the immobilized AuNPs increased the electron transfer rate at the SPE surface (Fig. 6a). The DNA biosensor response declined when higher amounts of AuNPs (i.e. more than 0.08 mg) were deposited on the electrode as the large excess of AuNPs on the SPE resulted in full surface coverage, which hindered the electron transfer reaction at the electrode surface.

The optimized AuNP-SPE was then further modified with the aminated HSiSs for DNA probe immobilization. The DNA biosensor response increased with increasing HSiS loading from 0.01 to 0.04 mg as the HSiSs increased the total surface area for binding with a large number of DNA probes, and this enhanced the DNA hybridization and intercalation reaction rates at the transducer surface (Fig. 6b). When the amount of the insulated HSiSs exceeded 0.04 mg on the AuNP-SPE, this caused sluggish electron transfer kinetics, and a lower DPV response.

The concentration of DNA probe loaded on the AuNP/HSiS-SPE was optimized between 0.5 and 6 μM. The DNA biosensor response increased with DNA probe loading from 0.5 to 2 μM DNA as the aminated HSiSs provided large loading capacity for immobilization of a higher amount of DNA probe, thereby increasing the DNA hybridization reaction rate [50]. The levelling off of the DPV response at a DNA probe concentration above 2 μM was attributed to the

Table 2 Electrodynamic data with regard to anodic peak potential (E_{PA}), cathodic peak potential (E_{PC}), potential difference (ΔE_P), anodic peak current (I_{PA}), cathodic peak current (I_{PC}) and anodic to cathodic peak current ratio (I_{PA}/I_{PC}) of $K_3[Fe(CN_6)]$ redox indicator with different surface-modified working electrodes

	E_{PA} (V)	E_{PC} (V)	ΔE_P (V)	I_{PA} (A)	I_{PC} (A)	I_{PA}/I_{PC}
Bare SPE	0.452	-0.073	0.525	5.508×10^{-4}	-5.965×10^{-4}	0.9234
AuNP-modified SPE	0.443	-0.054	0.497	9.236×10^{-4}	-9.591×10^{-4}	0.9630
HSiS-modified SPE	0.443	-0.153	0.596	4.443×10^{-4}	-1.987×10^{-4}	2.236
AuNP/HSiS-modified SPE	0.447	-0.049	0.496	9.194×10^{-4}	-9.580×10^{-4}	0.9597

AuNP gold nanoparticle, *HSiS* hollow silica sphere, *SPE* screen printed electrode

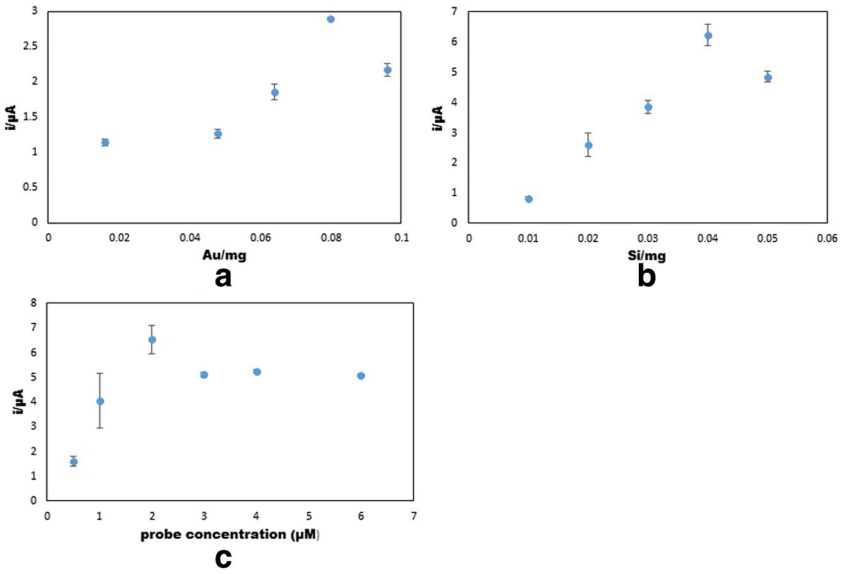

Fig. 6 Effect of gold nanoparticle (**a**), aminated hollow silica sphere (**b**) and DNA probe (**c**) loadings on the DNA biosensor response based on the intercalated anthraquinone-2-sulfonic acid monohydrate salt differential pulse voltammetry peak current signal

saturation of aminated HSiSs with DNA probe via glutaraldehyde cross-linking reaction. The dependence of the DNA biosensor response on DNA probe loading is illustrated in Fig. 6c.

Effect of DNA hybridization buffer solution

The buffer solution used for DNA hybridization assay was optimized in terms of buffer type, pH, buffer concentration and ionic strength to obtain the optimal DNA hybridization conditions to enhance the DNA hybridization rate of the DNA biosensor. The DNA biosensor showed the highest response to 1×10^{-8} μM cDNA with 1 mM anthraquinone redox intercalator in 0.05 M potassium phosphate buffer at pH 7 as it provided the most benign environment for DNA molecules compared with sodium phosphate and tris(hydroxymethyl)aminomethane hydrochloride buffer solutions (Fig. 7a). Hence, potassium phosphate buffer

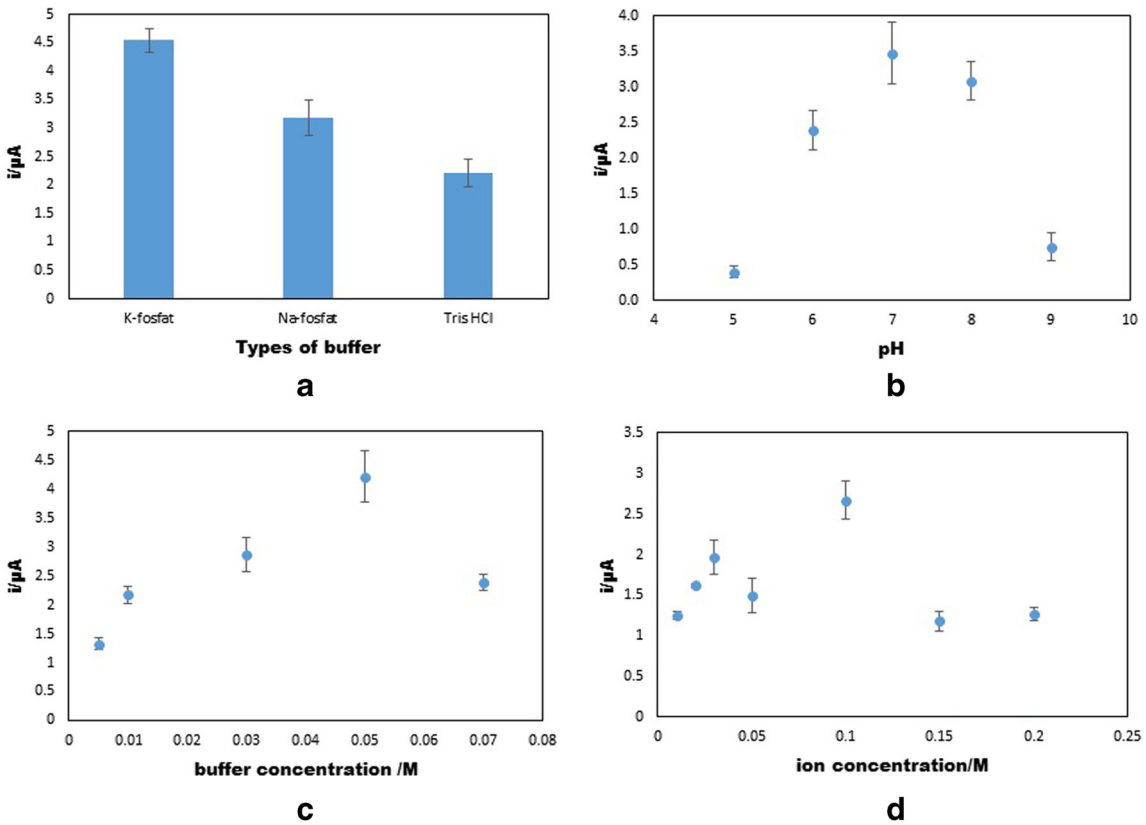

Fig. 7 Buffer solution (**a**), pH (**b**), buffer capacity (**c**) and ionic strength (**d**) profiles of the hollow silica sphere based DNA biosensor. Tris tris(hydroxymethyl)aminomethane

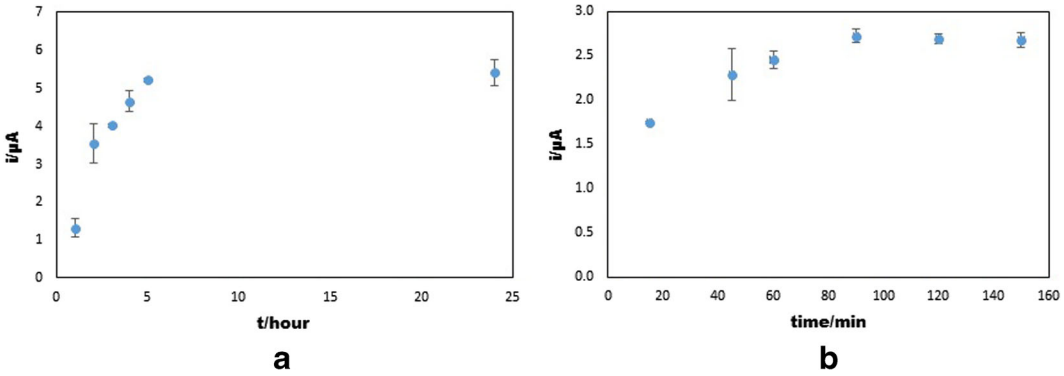

Fig. 8 DNA probe immobilization duration (**a**) and response time (**b**) of the DNA biosensor obtained with 1 mM anthraquinone-2-sulfonic acid monohydrate salt redox indicator

was used for further studies to maximize the DNA hybridization reaction.

The pH plays an important role in providing an appropriate environment for the DNA hybridization reaction [21, 49]. High or low pH may cause considerable denaturation of the duplex DNA [49]. As Fig. 7b shows, different pH environments caused large changes to the DNA hybridization process as illustrated by the significant DPV peak current change with pH. By reduction of the acidity (from pH 5 to pH 7) and alkalinity (from pH 9 to pH 7) of the 0.05 M potassium phosphate buffer, a maximum DPV signal was obtained at 3.46 μA. This clearly shows that a neutral environment made the DNA hybridization reaction more favourable. In an acidic environment, the DNA molecules become insoluble as a result of the protonation of the DNA phosphodiester bond, and that interfered with the DNA hybridization reaction [51], whereas in basic buffer solution, it broke up the weak hydrogen bonds between the DNA molecules, and denatured the helical double-stranded DNA (dsDNA) [52].

The potassium phosphate buffer capacity and ionic strength of the DNA hybridization buffer were then adjusted to reduce the steric hindrance and electrostatic repulsion between negatively charged phosphate groups of the immobilized dsDNA [53]. Potassium phosphate buffer at 0.05 M (Fig. 7.3c) containing 0.1 M K^+ ion (Fig. 7d) provided less steric repulsion and electrostatic interaction between negatively charged DNA molecules. The monovalent cation (i.e. K^+ ion) neutralized the negatively charged DNA sugar–phosphate backbone, and reduced the electrostatic repulsions between DNA molecules such that they can approach each other close enough to promote the DNA hybridization reaction [49]. In addition, the high salt content could also facilitate the stabilization of the DNA double helix configuration [54].

DNA immobilization and hybridization duration

Figure 8a shows the time taken for immobilization of the DNA probe on the immobilized aminated HSiSs. The DNA biosensor exhibited a higher DPV response as the glutaraldehyde-modified HSiS/AuNP-SPE was soaked in the DNA probe solution for a longer time of 1–5 h. This was because an extended immobilization time permitted a higher amount of DNA probes to be attached to the immobilized aminated HSiSs on the electrode, thereby resulting in a higher DNA hybridization reaction rate with the target DNA followed by accumulation of the AQMS redox label in the

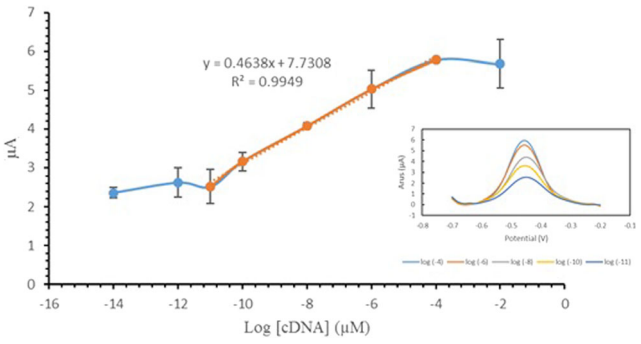

Fig. 9 Calibration curve of the aminated hollow silica sphere based *Escherichia coli* DNA biosensor generated by use of 1.0×10^{-14}–1.0×10^{-2} μM complementary DNA (cDNA) and 1 mM anthraquinone-2-sulfonic acid monohydrate salt at pH 7

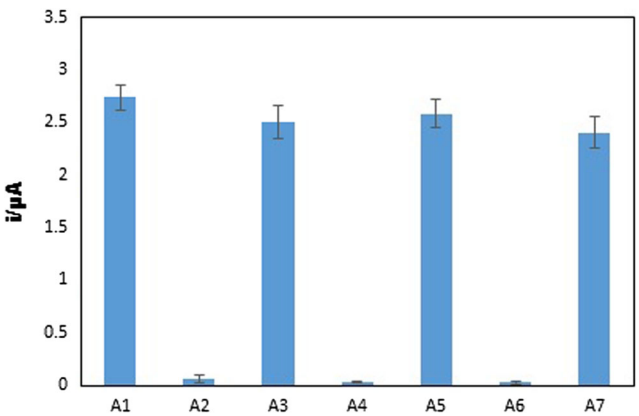

Fig. 10 Reversibility of the DNA biosensor with use of DNA rehybridization with 1.0×10^{-8} μM complementary DNA (30 min) (a1, a2, a3, a4) and 0.1 M NaOH regeneration solution (15 min) (b1, b2, b3)

Table 3 Analytical performance comparisons between the DNA biosensor developed and several reported electrochemical DNA biosensors for *Escherichia coli* detection

DNA supporter	Linear range (M)	LOD (M)	Reproducibility (RSD, %)	Hybridization time	Reference
AuNP/HSiS-modified SPE	1×10^{-17}–1×10^{-10}	1.74×10^{-18}	6.1	60 min	This work
AuNP/non-hollow silica sphere-modified screen-printed carbon electrode (control)	1×10^{-14}–1×10^{-8}	3.92×10^{-15}	–	60 min	This work
Graphene oxide/nickel ferrite/chitosan nanocomposite film	1×10^{-16}–1×10^{-6}	1×10^{-16}	–	30 s	[55]
Fe_2O_3@Au core–shell nanoparticles	1×10^{-13}–1×10^{-9}	0.01×10^{-12}	4.1	40 min	[56]
Screen-printed carbon paste electrode	5×10^{-10}–25×10^{-9}	1×10^{-11}	5.0	45 min	[2]
(3-Mercaptopropyl)trimethoxysilane 3D polymeric network-modified screen-printed Au electrode	21×10^{-12}–400×10^{-12}	6.3×10^{-12}	4.3	15 min	[57]
Alumina anodized oxide nanopore membrane	–	0.5×10^{-9}	–	–	[14]

AuNP gold nanoparticle, *HSiS* hollow silica sphere, *LOD* limit of detection, *RSD* relative standard deviation, *SPE* screen-printed electrode

immobilized dsDNA structure. After 5 h exposure to the DNA probe solution, the immobilized aminated HSiSs were saturated with DNA probes, and a steady-state DPV current was obtained.

DNA hybridization is the rate-limiting step that determines the in situ assay time. DNA hybridization was performed in a single step simply by the dipping of the DNA hybrid electrode into the cDNA solution at room temperature. The DNA biosensor response gradually increased with DNA hybridization time, which signifies increasing DNA duplex formation on the modified SPE, and demonstrated a 90-min DNA hybridization time (Fig, 8b). The DNA biosensor had a saturated response when the entire DNA recognition sites on the SPE had been completely hybridized with cDNA.

Analytical performance of the *E. coli* DNA biosensor

The DPV response of the 0.05M potassium phosphate buffer containing different molar concentrations of *E .coli* cDNA (1×10^{-14}–1×10^{-2} μM) and 0.1 M K^+ ion at pH 7 was measured with the DNA biosensor method to construct a linear calibration curve. The DNA biosensor demonstrated a linear response over a broad *E. coli* cDNA concentration range from 1×10^{-12} to 1×10^{-2} μM (Fig. 9) because of the hollow structure of the silica spheres with an inner void, which offered an efficient pathway for cDNA to diffuse into the biorecognition surface. The limit of detection of the *E. coli* DNA biosensor calculated on the basis of three times the standard deviation of the biosensor response in the linear range divided by the linear calibration slope was 1.74×10^{-12} μM [49].

The regeneration performance of the *E. coli* DNA biosensor is presented in Fig. 10. The response of the DNA biosensor decreased after it had been soaked in 0.1 M NaOH regenerating agent, which was ascribed to the potent alkaline solution, which broke up the hydrogen bonds between base pairs of the immobilized DNA double helices. This was because the reaction between the OH^- ion of NaOH and the hydrogen atoms of the DNA sugar–phosphate backbone caused the cleavage of dsDNA. However, the DNA biosensor response increased to the initial response after rehybridization with the target DNA, and the DNA biosensor response was regenerable over four successive regeneration and rehybridization cycles, with reversibility relative standard deviations in the range of 4–6% ($n = 4$).

Table 4 A comparison between electrochemical DNA biosensor and cultural method in the determination of *E.coli* DNA in water samples

Water Sample	DPV current signal (μA) (n=3)	t value cf baseline (t value > $t_{critical}$) ($t_{critical}$ =2.1318)	Bacteria culture on eosin methylene blue (number cfu/100 mL)
Buffer (baseline)	0.445±0.003	-	-
Langat River near University	0.404±0.230	1.922	0
Langat River near Factory	6.602±0.060	161.191	75-80
Langat River near Market	6.914±0.100	107.211	>80
Langat River near Restaurant	4.875±0.400	18.803	60-70

Table 3 summarizes the analytical properties of several reported DNA biosensing platforms, including the proposed AuNP/HSiS-SPE DNA hybrid supporter for *E. coli* detection and AuNPs/non-hollow silica spheres-modified screen-printed carbon electrode as a control. The DNA biosensor based on AuNP/HSiS hybrid material showed large improvements with respect to the dynamic linear response range and detection limit as compared with some other DNA carrier matrices, for example, graphene oxide/nickel ferrite/chitosan nanocomposite film [55], Fe_2O_3@Au core–shell magnetic nanoparticles [56], a screen-printed carbon paste electrode [2], a (3-mercaptopropyl)trimethoxysilane three-dimensional polymeric network [57] and an aluminium anodized oxide nanopore membrane [14]. This was attributed to the large specific surface area of the as-synthesized aminated HSiSs, which possessed a rather rough surface morphology that increased the DNA binding capacity. The high binding capacity of the HSiSs was the key feature in enhancing the sensitivity for *E. coli* DNA screening. The hollow structure of the HSiSs also served to increase the diffusion kinetics, thus shortening the diffusion time, and improving the electrochemical kinetics performance of the *E. coli* DNA biosensor.

E. coli detection from environmental samples

Electrochemical DNA biosensors were applied to detect the presence of *E. coli* in environmental water samples. Water samples were collected from various locations along Langat River and filtered through a 45-μm pore size filter to remove large, unwanted particles, and the samples were filtered again through a 0.2-μm filter. DNA was extracted from the samples by heating and sonication for 20 min. *E. coli* DNA was detected by amperometry. The numbers of *E. coli* were verified by a culture method. The results obtained by electrochemical detection and the culture method from the different samples are reported in Table 4. The water sample from Langat River obtained next to the market gave the highest response for the electrochemical method and the culture method. The water sample obtained next to the National University of Malaysia give almost no response for both methods. From the *t* test, the *t* values from the factory site, the market site and the restaurant site are higher than the *t* critical value with 90% confidence intervals.

Conclusion

The potential application of HSiSs for high DNA loading has been demonstrated. This DNA biosensor is capable of determining low DNA concentrations down to the attomolar level, and has excellent selectivity toward *E. coli* complementary sequence. The improved performance of the DNA biosensor is attributed to the hollow structure of the HSiSs, which not only provided a larger surface area for DNA binding but also facilitated diffusion of molecules in and out of the hollow particles. The proposed HSiSs may be applied for versatile immobilization of biomolecules and chemical reagents for various analytical purposes.

Acknowledgements We acknowledge the National University of Malaysia for providing grants GP-5179 and DPP-2016-064 and the Ministry of Science, Technology and Innovative Nanotechnology Directorate for grant NND/ND/(2)/TD11-009.

Compliance with ethical standards

Conflict of interest The authors declare that they have no competing interests.

References

1. Jiang X, Wang R, Wang Y, Su X, Ying Y, Wang J, et al. Evaluation of different micro/nanobeads as amplifiers in QCM immunosensor for more sensitive detection of *E. coli* O157:H7. Biosens. Bioelectron. 2008;29:23–8.
2. Paniel N, Baudart J. Colorimetric and electrochemical genosensors for the detection of *Escherichia coli* DNA without amplification in seawater. Talanta. 2013;115:133–42.
3. Ercole C, Cachio P, Botta CL, Centi V, Lepidi A. Bacterially induced mineralization of calcium carbonate: the role of exopolysaccharides and capsular polysaccharide. Microsc Microanal. 2007;13:42–50.
4. Sharma VK, Dean-Nystrom EA, Casey TA. Semi-automated flurogenic PCR assays (TaqMan) for rapid detection of Escherichia coli O157:H7 and other Shiga toxigenic *E. coli*. Mol Cell Probe. 1999;13:291–302.
5. Zelada-Guillen GA, Riu J, Duzgun A, Rios FX. Immediate detection of living bacteria at ultralow concentrations using a carbon nanotube based potentiometric aptasensor. Angew Chem Int Ed. 2009;48:7334–7.
6. Zhang GJ, Zhang L, Huang MJ, Luo ZHH, Tay GKI, Lim EA, et al. Silicon nanowire biosensor for highly sensitive and rapid detection of dengue virus. Sens Actuators B. 2010;146:138–44.
7. Lam SK, Devine PL. Evaluation of capture ELISA and rapid immunochromatographic test for the determination of Ig M dan Ig G antibodies produced during dengue infection. Clin Diagn Virol. 1998;(10):75–81.
8. Subramanian A, Irudayaraj J, Ryan T. A mixed self-assembled monolayer-based surface plasmon immunosensor for detection of E. coli O157:H7. Biosens Bioelectron. 2006;21:998–1006.
9. Li J, Tan W, Wang K, Xiao D, Yang X, He X, et al. Ultrasensitive optical DNA biosensor based on surface immobilization of molecular beacon by a bridge structure. Anal. Sci. 2001;17:1149–53.
10. Zhu D, Liu J, Tang Y, Xing D. A reusable DNA biosensor for the detection of genetically modified organism using magnetic bead-based electrochemiluminescence. Sens Actuators B. 2010;149:221–5.
11. Guo SH, Lin J, Penchev M, Yengel E, Ghazinejad M, Ozkan CS, et al. Label free DNA detection using large area graphene based field effect transistor biosensors. J Nanosci Nanotechnol. 2011;11:5258–63.

12. Karamollaoglu I, Oktem HV, Mutlu M. QCM-based DNA biosensor for detection of genetically modified organisms (GMOs). Biochem Eng J. 2009;44:142–50.
13. Wang J. Electrochemical nucleic acid biosensors. Anal Chim Acta. 2002;469:63–71.
14. Wang L, Liu Q, Hu Z, Zhang Y, Wu C, Yang M, et al. A novel electrochemical biosensor based on dynamic polymerase-extending hybridization for *E. coli* O157:H7 DNA detection. Talanta. 2009;78:647–52.
15. Li C, Chen X, Wang N, Zhang B. An ultrasensitive and label-free electrochemical DNA biosensor for detection of DNase I activity. RSC Adv. 2017;7:21666–70.
16. Evtugyn GA, Stepanova VB, Porfireva AV, Zamaleeva AI, Fakhrullin RR. Electrochemical DNA sensors based on nanostructured organic dyes/DNA/polyelectrolyte complexes. J Nanosci Nanotechnol. 2014;14(9):6738–47.
17. Teles FRR, Foncessca LP. Trends in DNA biosensors. Talanta. 2008;77:606–23.
18. Ulianas A, Lee YH, Ahmad M, Lau HY, Ishak Z, Tan LL. A regenerable screen-printed DNA biosensor based on acrylic microsphere-gold nanoparticle composite for genetically modified soybean determination. Sens Actuators B. 2014;190:694–701.
19. Liebana S, Brandao D, Cortes P, Campoy S, Alegret S, Pividori MI. Electrochemical genosensing of Salmonella, Listeria and Escherichia coli on silica magnetic particles. Anal Chim Acta. 2016;904:1–9.
20. Cai L, Chen ZZ, Dong XM, Tang HW, Pang DW. Silica nanoparticles based label-free aptamer hybridization for ATP detection using hoechst33258 as the signal reporter. Biosens Bioelectron. 2011;29:46–52.
21. B.H. Cha, S.M. Lee, J.C. Park, K.S. Hwang, S.K. Kim, J.J. Hong. Detection of hepatitis B virus (HBV) DNA at femtomolar concentrations using silica nanoparticle-enhanced microcantilever sensor. Biosens Bioelectron. 2009:25:130-5.
22. Xiao QG, Tao X, Zou HK, Chen JF. Comparative study of solid silica nanoparticles and hollow silica nanoparticles for the immobilization of lysozyme. Chem Eng J. 2008;137:38–44.
23. Li Y, Shi J. Hollow-structured mesoporous materials: chemical synthesis, functionalization and applications. Adv Mater. 2014;26: 3176–205.
24. J.F. Chen, H.M. Ding, J.X. Wang, L. Sao. Preparation and characterization of porous hollow silica nanoparticles for drug delivery application. Biomaterials. 2004:25:723-7.
25. Morey MS, O'Brien S, Schwarz S, Stucky GD. Hydrothermal and postsynthesis surface modification of cubic, MCM-48 and ultralarge pore SBA-15 mesoporous silica with titanium. Chem Mater. 2000;12(4):898–911.
26. Okada K, Shimai A, Takei T, Hayashi S, Yasumori A, Mackenzie KJD. Preparation of microporous silica from metakaolinite by selective leaching method. Microporous Mesoporous Mater. 1998;21: 289–96.
27. Lee B, Kim Y, Lee H, Yi J. Synthesis of functionalized porous silicas via templating method as heavy metal ion adsorbents: the introduction of surface hydrophilicity onto the surface of adsorbents. Microporous Mesoporous Mater. 2001;50:77–90.
28. He F, Zhuo RX, Liu LJ, Jin DB, Feng J, Wang XL. Immobilized lipase on porous silica beads: preparation and application for enzymatic ring-opening polymerization of cyclic phosphate. React Funct Polym. 2001;47(2):153–8.
29. Zhang Z, Dai S, Fan X, Blom DA, Pennycook SJ, Wei Y. Controlled synthesis of CdS nanoparticles inside ordered mesoporous silica using ion-exchange reaction. J Phys Chem B. 2001;105(29):6755–8.
30. Jain A, Rogojevic S, Ponoth S, Agarwal N, Matthew I, Gill WN, et al. Porous silica materials as low-k dielectrics for electronic and optical interconnects. Thin Solid Films. 2001;398-399:513–22.
31. R.K. Sharma, S. Das, A. Maitra, Enzymes in the cavity of hollow silica nanoparticles. J Colloid Interface Sci. 2005:284:358-61.
32. Bai Y, Yang H, Yang W, Li Y, Sun C. Gold nanoparticles-mesoporous silica composite used as an enzyme immobilization matrix for amperometric glucose biosensor construction. Sens Actuators B. 2007;124:179–86.
33. Chen Y, Chu C, Zhou Y, Ru Y, Chen H, Chen F, et al. Reversible pore-structure evolution in hollow silica nanocapsules: large pores for siRNA delivery and nanoparticle collecting. Small. 2011;20: 2935–44.
34. Li X, He G, Han Y, Xue Q, Wu X, Yang S. Magnetic titania-silica composite-Polypyrrole core-shell spheres and their sensitivity toward hydrogen peroxide as electrochemical sensor. J Colloid Interface Sci. 2012;387:39–46.
35. Ariffin EY, Lee YH, Futra D, Tan LL. Aminated hollow silica spheres for electrochemical DNA biosensor. AIP Conf Proc. 2015;1678:050008.
36. Solanki PR, Kaushik A, Chavhan PM, Maheshwari SN, Malhotra BD. Nanostructured zirconium oxide based genosensor for Escherichia coli detection. Electrochem Commun. 2009;11:2272–7.
37. Boissiere C, Lee AVD, Mansouri AE, Larbot A, Prouzet E. A double step synthesis of mesoporous micrometric spherical MSU-X silica particles. Chem Commun. 1999, 20:2047–8.
38. Zhang L, Foxman B, Gilsdorf JR, Marrs CF. Bacterial genomic DNA isolation using sonication for microarray analysis. Benchmarks. 2005;39(5):640–1.
39. Dashti AA, Jadaon MM, Abdulsamad AM, Dashti HM. Heat treatment of bacteria: A simple method of DNA extraction for molecular techniques. Kuwait Med J. 2009;41(2):117–22.
40. De Lange MF, Vlugt TJH, Gascon J, Kapteijn F. Adsorptive characterization of porous solids: Error analysis guides the way. Microporous Mesoporous Mater. 2014;200:199–215.
41. Zielinski JM, Kettle L. Physical characterization: surface area and porosity. London: Intertek; 2013.
42. Nguyen A-T, Park CW, Kim SH. Synthesis of hollow silica by Stöber method with double polymers as templates. Bull Korean Chem Soc. 2014;35(1):173–6.
43. Alqasaimeh M, Lee YH, Ahmad M, Raj ASS, Tan LL. A large response range reflectometric urea biosensor made from silica-gel nanoparticles. Sensors. 2014;14:13186–209.
44. Mourhly A, Khachanil M, Hamidi AE, Kacimi M, Halim M, Arsalane S. The synthesis and characterization of low-cost mesoporous silica SiO_2 from local pumice rock. Nanomater Nanotechnol. 2015;5(35):1–7.
45. Nakanishi K, Tomita M, Kato K. Synthesis of amino-functionalized mesoporous silica sheets and their application for metal ion capture. J Asian Ceram Soc. 2015;2015(3):70–6.
46. Sayen S, Walcariu A. Electro-assisted generation of functionalized silica films on gold. Electrochem Commun. 2003;5:341–8.
47. Monk PMS. Fundamentals of electro-analytical chemistry. New York: Wiley; 2001.
48. López-Paz JL, González-Martínez MA, Escorihuela J, Banuls MJ, Puchades R, Maquieira A. Direct and label-free monitoring oligonucleotide immobilization, non-specific binding and DNA biorecognition. Sens Actuators, B. 2014;192:221–8.
49. Ulianas A, Lee YH, Sharina AH, Tan LL. An electrochemical DNA microbiosensor based on succinimide-modified acrylic microspheres. Sensor. 2012;12:5445–60.
50. Kerman K, Morita Y, Takamar Y, Ozsos M, Tamiya E. Modification of Escherichia coli single-stranded DNA binding protein with gold nanoparticles for electrochemical detection of DNA hybridization. Anal Chim Acta. 2004;510:169–74.
51. Hames BD, Higgins SJ. Nucleic acid hybridisation-a practical approach. New York: Oxford University Press; 1985. p. 78.
52. Okahata Y, Kawase M, Niikura K, Ohkate F, Furusawa H, Ebara Y. Kinetic measurements of DNA hybridization on an

oligonucleotide-immobilized 27-MHz quartz crystal microbalance. Anal Chem. 1998;70:1288–96.
53. Gooding JJ. Electrochemical DNA hybridization biosensors. Electroanalysis. 2002;14(17):1149–56.
54. Luracelli F, Marrazza G, Turner APF, Mancini M. Carbon and gold electrodes as electrochemical transducers for DNA hybridization sensors. Biosens Bioelectron. 2004;19:515–30.
55. Tiwari I, Singh M, Pandey CM, Susana G. Electrochemical detection of a pathogenic *Escherichia coli* specific DNA sequence based on a graphene oxide-chitosan composite decorated with nickel ferrite nanoparticles. RSC Adv. 2015;5:67115–24.
56. Li K, Lai Y, Zhang W, Jin L. Fe_2O_3@Au core/shell nanoparticle-based electrochemical DNA biosensor for Escherichia coli detection. Talanta. 2011;84:607–13.
57. Marugan JR, Dominguez MDP, Casero E, Vazquez L, Garcia T, Alfambra AMP, et al. Sol-gel derived gold nanoparticles biosensing platform for *Escherichia coli* detection. Sens Actuators B. 2013;182:307–14.